Inside a Collapsing Bubble: Sonoluminescence and the Conditions During Cavitation

Kenneth S. Suslick[1] and David J. Flannigan[2]

[1]School of Chemical Sciences, University of Illinois at Urbana-Champaign, Urbana, Illinois 61801; email: ksuslick@uiuc.edu

[2]California Institute of Technology, Pasadena, California 91125; email: flanniga@caltech.edu

Annu. Rev. Phys. Chem. 2008. 59:659–83

First published online as a Review in Advance on December 11, 2007

The *Annual Review of Physical Chemistry* is online at http://physchem.annualreviews.org

This article's doi: 10.1146/annurev.physchem.59.032607.093739

0066-426X/08/0505-0659$20.00

Key Words

sonochemistry, hydrodynamics, ultrasound, plasma, optical emission spectroscopy

Abstract

Acoustic cavitation, the growth and rapid collapse of bubbles in a liquid irradiated with ultrasound, is a unique source of energy for driving chemical reactions with sound, a process known as sonochemistry. Another consequence of acoustic cavitation is the emission of light [sonoluminescence (SL)]. Spectroscopic analyses of SL from single bubbles as well as a cloud of bubbles have revealed line and band emission, as well as an underlying continuum arising from a plasma. Application of spectrometric methods of pyrometry as well as tools of plasma diagnostics to relative line intensities, profiles, and peak positions have allowed the determination of intracavity temperatures and pressures. These studies have shown that extraordinary conditions (temperatures up to 20,000 K; pressures of several thousand bar; and heating and cooling rates of $>10^{12}$ K s^{-1}) are generated within an otherwise cold liquid.

INTRODUCTION

Sonochemistry: chemical reactions driven by sound or ultrasound, usually through the process of acoustic cavitation in a liquid, a liquid slurry, or at a liquid-solid/gas interface

SL: sonoluminescence

Cavitation: the formation, growth, oscillation, and collapse of bubbles in a liquid

Multibubble sonoluminescence (MBSL): emission of light from a large number of acoustically driven bubbles

Single-bubble sonoluminescence (SBSL): emission of light from a single solitary acoustically driven bubble

The irradiation of a liquid with sound of sufficient pressure causes the formation and oscillation of bubbles. This process, known as acoustic cavitation, is the root cause of sonochemistry and sonoluminescence (SL) (1–3). Within a broad parameter space, bubbles can be driven into highly nonlinear oscillations characterized by a slow volume growth followed by compression and a runaway implosion. It is around the point of maximum implosion that chemical reactions occur and light emission is observed. The bubble spends only ~0.003% of one period at its minimum size, but this spatiotemporal region represents the extreme conditions of cavitation.

Initial SL studies focused on the light generated from a cloud of cavitating bubbles formed in an ultrasonic field with a frequency generally from 20 kHz to 2 MHz. Marinesco & Trillat (4) first observed this process, known as multibubble sonoluminescence (MBSL), indirectly in 1933 when they noted the fogging of a photographic plate immersed in a water bath irradiated with high-intensity ultrasound. Although it was initially thought that the plate was fogged by a direct interaction of the silver halide crystals with the ultrasonic waves, Frenzel & Schultes (5) later directly observed luminescence within the bulk of the ultrasonically irradiated water. Since this time, researchers have devoted much work to elucidating the underlying physical and chemical processes responsible for SL.

Early studies of MBSL were nearly always conducted in aqueous solutions (6). Analyses of such spectra revealed that the SL consisted mainly of a broad and featureless continuum stretching across the visible region. In addition, excited-state emission bands of hydroxyl radicals (OH^*) were observed, indicating the dissociation of water molecules during cavitation. Besides spectroscopic analyses, many correlational studies were also conducted on MBSL (7), for example, light intensity as a function of external parameters such as bulk liquid temperature, the nature of the gas dissolved into the liquid, and properties of the applied acoustic field. These studies helped determine that the SL was sensitively dependent on the thermodynamic properties of the intracavity gas and vapor, suggesting that the light emission arose from compressional heating of the bubble contents. Quantifying the conditions generated during cavitation was also an early goal of researchers in physical acoustics (8–10). The first studies attempted to quantify the intracavity conditions by modeling SL as if it were blackbody radiation, although the mechanisms responsible for light emission were not known (11).

MBSL from nonaqueous liquids (12) revealed a spectral richness not previously observed. Emission bands and lines from electronically excited molecules and atoms observed during the sonication of organic solvents provided a great deal of information regarding the mechanisms at work and the conditions generated (13). Observation of discrete and easily identifiable molecular and atomic emission bands and lines provided multiple systems for which quantitative conditions could be measured from the relative intensities of vibronic and atomic bands (14, 15). In addition, analyses of the peak positions and profiles of atomic emission lines provided a means to estimate the intracavity densities and pressures during cavitation (16).

Soon after MBSL studies in nonaqueous liquids were reported, the SL from a single solitary bubble [single-bubble sonoluminescence (SBSL)] in water and

water/glycerine solutions was broadly reported, which also drew much attention (17, 18). Early SBSL studies suggested extreme energy focusing and the generation of potentially very high temperatures and pressures with the consequence of diverse and often exotic (and occasionally wild) hypotheses concerning the origins of the light emission. Although there was immediate interest in quantifying the conditions during SBSL from water, the spectra were simply not amenable to the same techniques employed for MBSL. Aqueous SBSL spectra were completely devoid of any features that would allow for quantitative analysis (19, 20). Remarkably, water remained the liquid of choice for SBSL studies for nearly a decade. Similar to the case for MBSL, studies of SBSL in liquids other than water provided additional information that allowed a better understanding of the conditions generated. The emission spectra from aprotic organic liquids (21) as well as concentrated mineral acids (22) contained discrete bands and lines, thus allowing the quantification of the SBSL temperatures and pressures (23).

P_a: applied acoustic pressure

In this review, we discuss many recent developments in the quantitative determination of the conditions generated during SL via analyses of the observed emission lines. We begin with a brief overview of the bubble dynamics that lead to light emission and the generation of extreme conditions. This is followed by a discussion of MBSL and the methods with which effective temperatures and pressures are determined. We then close with a discussion of the recent developments of the study of SBSL.

DYNAMICS OF ACOUSTICALLY DRIVEN BUBBLES

Description of Bubble Dynamics

One can quantitatively describe acoustic cavitation in a liquid irradiated with ultrasound with excellent accuracy throughout nearly all the process of formation, growth, and compression. Only in the last stage of collapse does theoretical description of the implosive collapse of bubbles become problematic, but of course everything of interest occurs only in the last stage of collapse! At relatively low applied acoustic pressures (P_a), the radial motion of a bubble in the sound field is linear. That is, as the pressure wave of the acoustic field having a sinusoidal waveform oscillates between compression and rarefaction, the radial motion of the bubble responds in kind. During rarefaction, the bubble volume increases due to the drop in pressure in the surrounding liquid. As the sound field turns to compression, the bubble volume decreases due to the rise in pressure. The linear motion of the bubble is therefore characterized by nearly equal rates of expansion and contraction with no shift in phase relative to the sound field. In fact, bubble expansion is slightly larger than bubble compression in this regime, simply because the surface area on expansion (and therefore gas flow in) is slightly larger than the surface area on compression (and gas flow out); this growth process for long-lived bubbles is called rectified diffusion (24, 25). This type of radial bubble motion does not show SL, as the relatively slow velocity of the interface and small degree of volume contraction do not rapidly compress the intracavity gas and vapor.

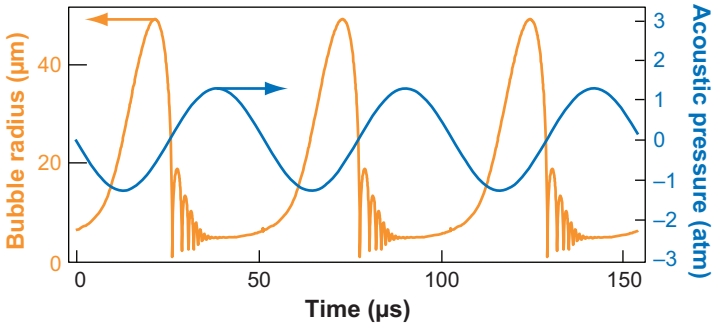

Figure 1

Calculated radial response of a bubble driven by a sinusoidal acoustic field. The bubble is assumed to be in equilibrium with respect to mass transport across the interface (i.e., no net change in intracavity mass over any single acoustic cycle). Thus, the bubble revisits the same spatial parameter space and shows no phase shift from one cycle to the next.

At elevated P_a, bubble motion becomes highly nonlinear (**Figure 1**) (24–26). This motion differs from linear bubble motion in many respects. To understand the nonlinear motion and to gain some feeling of the potential effects, we begin with a bubble at rest having a radius R_0. This is the radius at ambient conditions. As the acoustic pressure wave enters the rarefaction phase, the bubble begins a relatively slow volume growth. This volume growth is essentially linear for much of the time, and the total growth process lasts for roughly half the cycle. As the acoustic pressure wave enters its compression phase, at large P_a the bubble motion strongly deviates from the linear compression observed at lower P_a. The bubble continues to expand inertially, even though the compression phase of the acoustic cycle has begun. This system configuration is energetically unfavorable, however, and the bubble growth is quickly arrested (**Figure 1**) (at R_{max}, i.e., the maximum bubble radius). The bubble now begins a rapid and eventually runaway collapse. The velocity of this collapse in its last stages can be enormous and in some instances can be several times the speed of sound in gas at ambient temperature and pressure (27, 28). As the compression phase of the acoustic field continues, the bubble rapidly passes through R_0 on its way to R_{min}, the minimum bubble radius. As mentioned above, it is around R_{min} that high-energy chemical reactions and light emission occur. Because the gas and vapor are strongly compressed at R_{min}, the bubble quickly rebounds and expands. The bubble then goes through a series of secondary compressions and expansions of diminishing amplitude at roughly the Minnaert frequency (24, 25) until finally coming to rest again at R_0. For a bubble that is in equilibrium with respect to mass transport (**Figure 1**), the same radial motion is repeated almost exactly from one cycle to the next for an isolated bubble far from any surface or interface. Single-bubble cavitation can show remarkable stability and has a phase jitter of ~1 ppm (i.e., 50 ps on a cycle time of 50 μs) (18, 20). This type of motion is typical of SBSL. For MBSL, the situation is more complex, and a large percentage of the bubbles composing the cavitation cloud undergo transient cavitation. During transient cavitation, the bubble may oscillate for as little as one acoustic cycle before catastrophically imploding and fragmenting.

R_0: bubble radius at ambient conditions

Minnaert frequency: the resonant frequency of a bubble at which it will vibrate after being subjected to an impulsive force, assuming the gas within the bubble is compressed adiabatically

Rayleigh-Plesset Equation

One can model the radial motion of an acoustically driven bubble using any family of equations related to the Rayleigh-Plesset equation (RPE). RPEs can vary in complexity and have been built up with contributions from many researchers over the past century (24, 25, 29, 30). An example of an RPE is shown in Equation 1:

Rayleigh-Plesset equations (RPEs): equations describing the oscillation of an acoustically driven bubble

$$R\ddot{R} + \frac{3}{2}\dot{R}^2 = \frac{1}{\rho}\left[\left(P_0 + \frac{2\sigma}{R_0}\right)\left(\frac{R_0}{R}\right)^{3\gamma} - \frac{2\sigma}{R} - \frac{4\mu\dot{R}}{R} + P_\infty\right], \quad (1)$$

where R is the bubble radius [the overdots signify first (velocity) and second (acceleration) derivatives of the interface with respect to time], R_0 is the bubble radius at ambient conditions, ρ is the bulk liquid density, P_0 is the ambient liquid pressure, σ is the surface tension, μ is the shear viscosity, and P_∞ is the far-field acoustic pressure (but see 29). The left-hand side of Equation 1 describes the inertial characteristics of the bubble interface, and equating this to $\frac{P_L - P_\infty}{\rho}$, where P_L is the pressure in the liquid at the bubble wall, gives the fundamental equation of bubble dynamics. The term $(P_0 + \frac{2\sigma}{R_0})(\frac{R_0}{R})^{3\gamma}$ represents the intracavity gas pressure as the bubble radius varies from R_0 to R. RPEs work well over most of the range of bubble motion; any RPE assumes, however, that the density of the liquid is very large compared with the density of the gas within the bubble. This assumption fails in the case of a strongly driven bubble as it rapidly approaches its minimum radius.

MULTIBUBBLE SONOLUMINESCENCE

One can generate MBSL by irradiating a gassy liquid with ultrasound, typically pitched at a few tens to a few hundreds of kilohertz at an acoustic power of several watts per square centimeter. **Figure 2*a*** shows an image of a cloud of sonoluminescing bubbles generated by a 20-kHz titanium horn (which is a resonant frequency driven by a piezoceramics stack; the motion of the horn tip is typically a few tens of micrometers). The cloud consists of a large number of bubbles distributed fairly uniformly around the horn tip; the cloud itself can undergo substantial dynamic behavior on the time frame of seconds and is strongly dependent on the applied acoustic pressure (31). Because of the spatial distribution, the actual acoustic pressure felt by each bubble in the field is not uniform, and the range of bubble dynamics is broad. The result is a wide range in the number of photons per bubble collapse. **Figure 2*a*** qualitatively illustrates this effect. This further suggests that the intracavity conditions also vary depending on the spatial location of the bubbles relative to the acoustic source. At present, quantification of the intracavity conditions as a function of spatial location within the bubble cloud has not been accomplished.

MBSL from a large number of liquids has been reported, and spectral analyses of the emitted light have revealed a strong dependence on the choice of liquid. As noted above, MBSL spectra from aqueous solutions generally show weak and broadened OH^* emission atop a featureless continuum with little else. Spectroscopic studies of MBSL generated in nonaqueous liquids proved much more fruitful. For example, the MBSL spectra from *n*-alkanes saturated with noble gas comprise $C_2{}^*$, C_2H^*, and CH^*

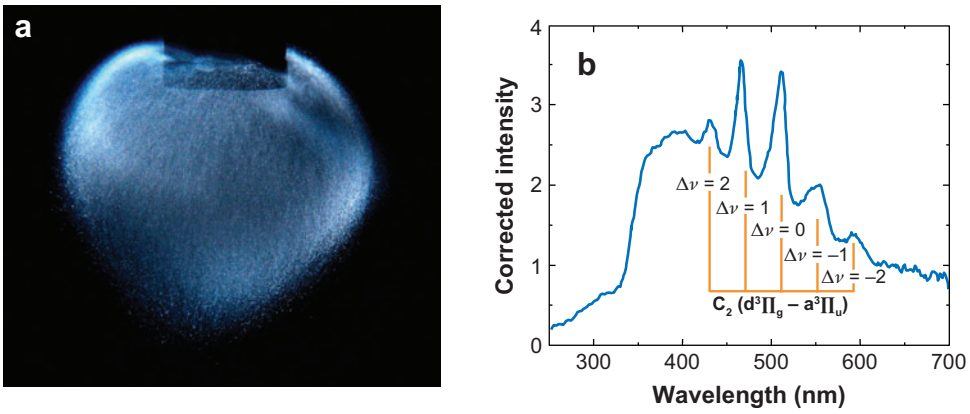

Figure 2

(*a*) True-color photograph (no external lighting) of a cloud of sonoluminescing bubbles generated with an ultrasonic horn in 96 wt% H_2SO_4 saturated with Xe gas. The diameter of the Ti horn tip is 1 cm. Photograph courtesy of N.C. Eddingsaas. (*b*) Multibubble sonoluminescence spectrum generated from the sonication of Ar saturated dodecane at 4 °C. The emission is assigned to the Swan band of C_2, and the transitions responsible for each line are shown.

emission bands, whereas those from *n*-alkanes containing nitrogen or oxygen show CN^*, CO_2^*, and OH^* emission bands (13). All MBSL spectra show an underlying continuum (which can be weak or strong relative to the band emission, depending on the system), regardless of the particular liquid employed. Spectroscopic studies have indicated that the continuum is most likely molecular in origin, analogous to the continuum observed in hydrocarbon flames (32, 33). Recent work in mineral acids, however, has shown that the origin of the continuum, at least in these aqueous liquids, is likely a combination of molecular and plasma processes (31). Although the precise mechanisms at work are still debated, clearly much has been learned about the processes at work by studying SL from liquids other than pure water. More importantly, the observation of discrete emission bands and lines provides a means with which to quantify the effective temperatures and pressures generated during MBSL.

Conditions During Multibubble Acoustic Cavitation

The extreme conditions generated during acoustic cavitation are such that homolytic bond cleavage is significant. This process is known as sonochemistry and has been employed to dramatically increase reaction rates of mixed-phase reactions (especially liquid-solid reactions of reactive metals), to synthesize nanostructured inorganic materials, and to remediate contaminated water (1, 3, 34, 35). New and fascinating discoveries are still being made in the area of sonochemistry and more generally mechanochemistry (i.e., chemical reactions driven by mechanical action). For example, mechanical forces applied to polymers by acoustic cavitation can be used to

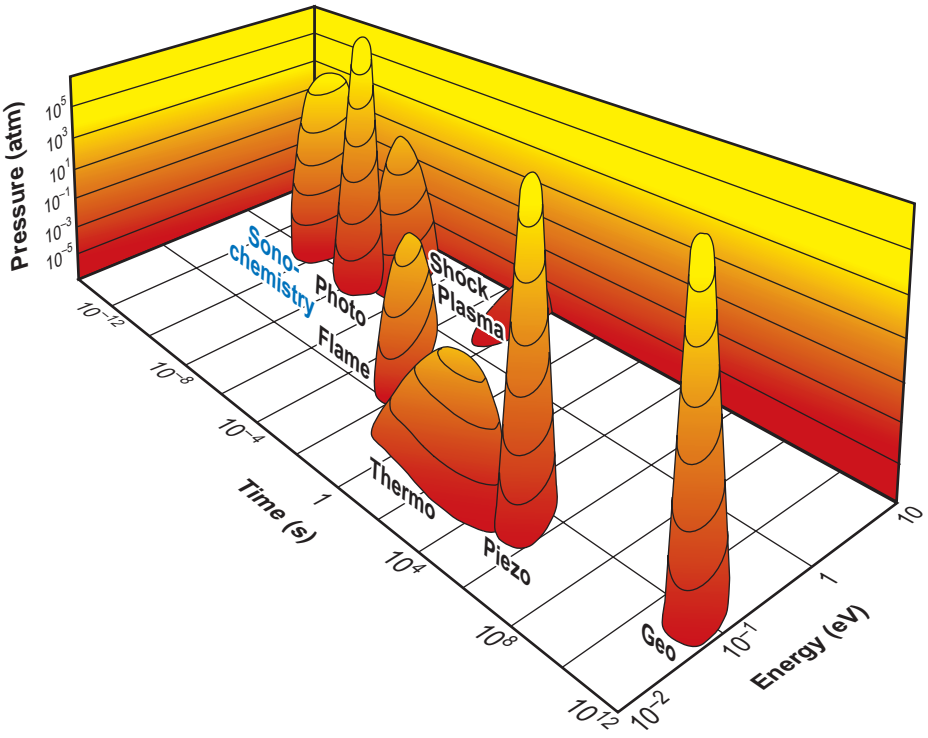

Figure 3

Chemistry is, fundamentally, the interaction of energy and matter. The parameters that control that interaction are the amount of energy per molecule, the time of the interaction, and the pressure under which that interaction occurs. This schematic represents the distinct domains of chemistry. Acoustic cavitation and its consequent sonochemistry provide an unusual method to access a unique parameter space for exploring new and interesting chemistry and physics.

direct reactions along specific potential energy surfaces (36). Work from our group on cavitation-induced interparticle collisions has advanced the understanding of the external effects of cavitation (37–39), as well as the molecular-level mechanisms of mechanoluminescence (40, 41). Indeed, acoustic cavitation provides a unique means for driving a wide variety of reactions, generating products not typically accessible by other standard means (**Figure 3**).

Temperatures During Multibubble Cavitation by Kinetic Measurements

Initial studies on quantifying the temperatures generated during acoustic cavitation exploited sonochemistry via a method termed comparative-rate thermometry (42). The sonication of a liquid of known composition, analysis of the sonolysis products, and determination of rate constants for specific kinetic pathways allowed for

temperature determination via the Arrhenius relation. For example, by sonicating solutions of volatile metal carbonyls in mixtures of *n*-alkanes containing an excess of triphenylphosphine and observing the first-order rates of ligand exchange, Suslick and coworkers (42) found that there are two sites of significant sonochemical activity: an initially gas-phase site (the majority) and an initially liquid-phase site (the minority). The hot intracavity gas-phase reaction zone had an effective temperature of 5200 ± 650 K, whereas an initially liquid phase (either the bubble shell or microdroplets injected into the hot core) was ~1900 K. These results supported other qualitative studies that also suggested the presence of two distinct sites of sonochemical activity based on observed sonolysis products (6, 43). Calculations together with recent experimental evidence suggest that the role of the bubble interfacial surface is minimal relative to microdroplet injection (44, 45).

Other kinetic studies have attempted to make use of a method known as the methyl radical recombination technique (46, 47). This method uses the sonochemical generation of methyl radicals and their subsequent recombination and loss of H_2 to form acetylene (C_2H_2), ethylene (C_2H_4), and ethane (C_2H_6). In principal, one can use the ratio of the sum of the observed energy yields (*G*, moles of product per joule of absorbed acoustic energy) of C_2H_2 and C_2H_4 to the observed *G* of C_2H_6 to estimate an effective intracavity temperature. Because of the dynamic and highly reactive environment within the bubble, however, this approach must make significant assumptions (48–50). It is assumed, for example, that C_2H_2, C_2H_4, and C_2H_6 are exclusively formed via specific reaction pathways without contributions from other mechanisms. Even more worrisome, it is assumed that these small molecules themselves do not undergo sonolysis (i.e., the formation of ethane, ethylene, and acetylene is irreversible). Regardless, reasonable temperatures ranging 2000 to 5000 K have been estimated via this method.

As with all measurements during multibubble cavitation or MBSL, the measured temperatures are effective temperatures only (33, 51, 52); due to the spatial distribution of bubbles and the distribution in the acoustic pressures to which they are subjected, the conditions created are not identical in each bubble in the cloud. In fact, one does not even have a good grasp on the overall number of bubbles composing the cavitation cloud, much less the number undergoing implosive collapse (i.e., the number of microreactors) at any given time. Significant experimental efforts, however, are being made toward the goal of a more detailed understanding of cavitating bubble clouds (53–56). Of course, another approach to overcome the limitations of variations in bubble cloud population and distribution is simply to abandon the cloud in favor of quantifying the production of photons, radicals, and ions during acoustic cavitation of a single, solitary bubble in water (57); we address the determination of intracavity conditions during SBSL below.

Temperatures During Multibubble Sonoluminescence by Spectroscopic Measurements

Spectroscopic methods have become a formidable method of quantifying the temperatures generated during MBSL. These methods have exploited the dependence

of the internal (i.e., bound) population distribution on temperature for thermally equilibrated systems; by comparing the relative intensities of emission lines from electronically excited atoms and molecules, one can determine an effective emission temperature. This is the same technique employed to quantify the thermal conditions of high-temperature sources (e.g., plasmas and flames) and remote locations (e.g., stellar surfaces). Of course, this technique is limited by the simple necessity of observing discrete emission lines in the SL spectra. MBSL spectra typically contain emission lines and therefore are quite amenable to this technique. We note that other spectrometric methods of pyrometry that use continuous radiative transitions rather than discrete transitions are highly model dependent (i.e., blackbody and bremsstrahlung).

Bremsstrahlung: electromagnetic radiation produced by the acceleration of a charged particle via interaction with another particle

We can describe the intensity of an emission line occurring from relaxation (induced as well as spontaneous) of an electronically excited atom by (58)

$$I_{nm} = \frac{hc}{4\pi} \cdot l \cdot \rho_o \cdot \frac{g_n}{Q} \cdot \frac{A_{nm}}{\lambda_n} \cdot \exp(-E_n/kT). \quad (2)$$

Here, h is Planck's constant, c is the speed of light, k is the Boltzmann constant, l is the path length of the confining region, ρ_o is the atom number density, g_n is the degeneracy of the upper state n, Q is the partition function ($\sum_n g_n \exp(-E_n/kT)$), A_{nm} is the Einstein transition probability between states n and m, E_n is the energy of the upper state n, and T is the absolute temperature. In principle, one can determine temperatures by comparing calculated calibration curves (i.e., I_{nm} versus T) and experimental spectral measurements of absolute line intensity for a specific transition (provided self-absorption is not greater than ~1%). In addition to requiring careful measurements of line intensities, knowledge of path length and atom number density, and accurate spectroscopic constants, this method of single-line radiance pyrometry also has an effective temperature determination limit that is intrinsic to the species studied. Above a certain temperature specific to the line studied, the radiance of the line no longer increases owing to the counterbalancing of the population of the excited state by ionization. For example, the temperature limit for the Ar 415.8-nm line is ~16,000 K (59).

Compared with the single-line method, the two-line radiance ratio method is simpler because it eliminates the need to know the path length and atom number density. Furthermore, one needs to know only the relative Einstein transition probabilities. This is a significant point because the absolute transition probabilities are typically known only to within ~20% for even the most rigorously studied atomic transitions. An obvious requirement for the use of this method is that the system studied must show a Maxwell-Boltzmann distribution. Gas temperatures are then determined by measuring the relative populations of two or more states and determining the temperature that best fits the data. In addition to the two-line radiance ratio method, several other methods use this principle, such as atomic and molecular Boltzmann plots and the iso-intensity method.

We can derive the ratio of the intensities of two emission lines from Equation 2 and write it as

$$\frac{I_1}{I_2} = \frac{g_1 A_1 \lambda_2}{g_2 A_2 \lambda_1} \exp[(E_2 - E_1)/kT], \quad (3)$$

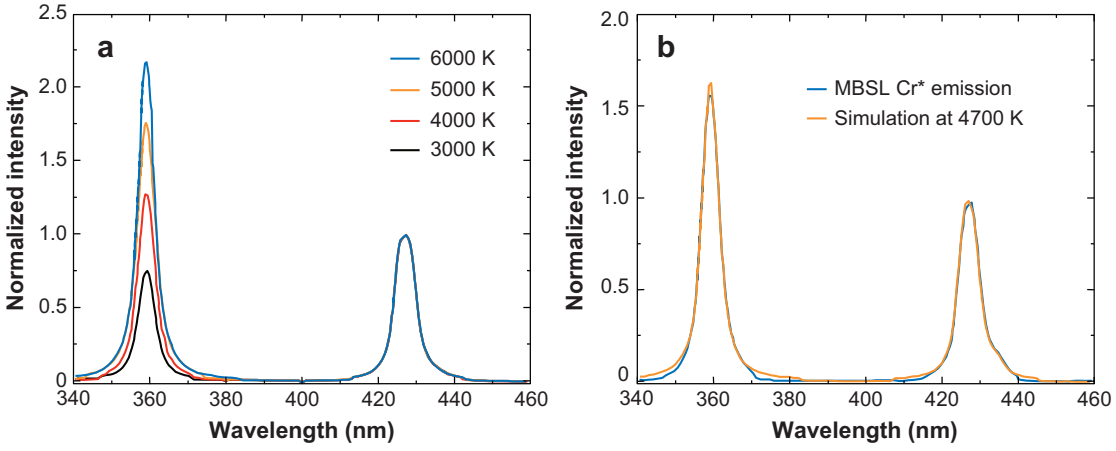

Figure 4

(*a*) Simulations of thermally equilibrated emission from Cr* atoms. The simulated spectra have been normalized to the peak intensity of the convoluted triplet at 424 nm. (*b*) Multibubble sonoluminescence (MBSL) from a solution of $Cr(CO)_6$ in silicone oil saturated with Ar gas, compared with a simulation at 4700 K. The underlying continuum was subtracted from the MBSL spectrum for clarity.

where the subscripts refer to the two spectral lines being compared. If the constants for a particular atom (i.e., g, A, λ, and E) are known fairly accurately, then one can determine an absolute temperature by measuring the relative intensities of two emission lines arising from transitions originating from different excited states (preferably well separated in energy). If the two lines used are from a neutral atom, the determined emission temperature reflects an atomic excitation temperature. In other words, the temperature corresponds to the equilibrium population among the excited states of the atom studied.

Our group has successfully used the two-line radiance ratio method in MBSL studies to determine the effective temperatures generated during acoustic cavitation. Sonication of solutions of volatile metal carbonyls in *n*-alkanes or silicone oil results in homolytic cleavage of the relatively weak metal-carbon bond resulting in free metal atoms (60). Electronic excitation and subsequent radiative relaxation of the metal atoms lead to the observation of intense and well-resolved emission lines in the MBSL spectra (61). One can then use the relative ratios of these emission lines to determine an effective MBSL temperature (14). **Figure 4** shows the emission lines observed from chromium atom excited states (i.e., Cr*) during the sonication of a solution of $Cr(CO)_6$ dissolved in silicone oil saturated with Ar and irradiated at 20 kHz. By using the two-line radiance ratio method and comparing the MBSL emission with simulated emission spectra at various temperatures, we found the effective MBSL temperature to be 4700 $\pm$ 300 K. Using the same method for other metal carbonyls also revealed temperatures of ~5000 K: Fe gave 5100 $\pm$ 300 K, and Mo gave 4800 $\pm$ 400 K. MBSL temperatures determined in this manner compare well with the emission temperature of 5100 $\pm$ 200 K determined by simulating the C_2

emission bands observed during sonication of low-volatility *n*-alkanes (12, 15), as well as the kinetic methods described above.

Polytropic ratio: ratio of the heat capacity at constant pressure to the heat capacity at constant volume

Pressure During Multibubble Sonoluminescence

As discussed above, the forceful implosion of an acoustically driven bubble leads to the generation of high intracavity temperatures and therefore also high pressures. The velocity of the imploding interface can become so rapid that the intracavity contents are heated nearly adiabatically and compressed to densities that might even approach the van der Waals hard core. As a starting point to gain a general idea of the pressures generated during cavitation, one can use a simple model of adiabatic changes in a state of an ideal gas. Because it is standard to use bubble radii and not volume within the field of acoustic cavitation, we write the expressions for reversible adiabatic compression as

$$T_f = T_i \left(\frac{R_i}{R_f} \right)^{3(\gamma-1)}, \tag{4}$$

$$P_f = P_i \left(\frac{R_i}{R_f} \right)^{3\gamma}, \tag{5}$$

where T_i and T_f are the initial and final temperatures, P_i and P_f are the initial and final pressures, R_i and R_f are the initial and final bubble radii, respectively, and γ is the ratio of heat capacities (i.e., polytropic ratio). By substituting the MBSL temperature determined from Cr* emission lines (4700 K), assuming an initial temperature of 298 K, and taking γ to be 1.67 for an Ar atmosphere, we find that the compression ratio (R_i/R_f) is 3.94. Substituting this into Equation 5 and assuming an initial pressure of 1 atm, we estimate that the final pressure reaches ~1000 atm. Although this is a simple model, it does give an impression as to the high pressures generated during cavitation.

One can determine the intracavity pressures generated during MBSL by again using emission lines from electronically excited atoms (16). Rather than using the line intensities (as for temperature determinations), we use the peak shifts to determine pressures. Perturbations of the energy levels of radiating species as well as reductions in the excited-state lifetimes owing to an increase in the collisional frequency with other species lead to shifts in peak positions and broadening of line profiles (i.e., uncertainty principle broadening) (58, 62, 63). By quantifying the various factors that lead to changes in line positions and profiles (e.g., Doppler effects, instrument contributions, and pressure broadening), one can determine an overall pressure at some specific temperature. We note that in a plasma, the contribution to the line profile from Stark effects and (to a lesser extent) ion broadening must also be considered (64), as discussed below.

Suslick and coworkers (16) experimentally determined the pressures generated during MBSL by quantifying the peak shifts in the emission lines from Cr* during the sonication of solutions of silicone oil saturated with He or Ar and containing $Cr(CO)_6$. During this work, the authors discovered that using emission line widths to determine MBSL pressures was not without complication; scattering of the emitted light by the bubble cloud caused significant experimental broadening of the Cr*

lines, which contributed up to 50% to the total line width. Thus they determined that pressure estimates from the emission line widths observed during MBSL were not reliable. The line shifts, however, were independent of the light-scattering effects of the bubble cloud. Theory on the behavior of the peak positions of emission lines of transition-metal atoms has not advanced to the point at which pressures can be determined in this manner a priori. Quantitative determinations, however, can be made by comparing MBSL emission line positions with those observed from ballistic compressors, the conditions within which approximate the conditions during acoustic cavitation. Because reliable high-pressure data for Cr* emission lines exist in the literature (65), we can make direct comparisons with MBSL Cr* emission lines. **Figure 5*a*** illustrates the red shift of each Cr* emission line comprising the triplet centered at ~27,800 cm^{-1} as a function of Ar bath gas pressure at a fixed temperature of 3230 K. **Figure 5*b*** shows the MBSL Cr* emission lines compared with the spectrum from a hollow cathode lamp. By comparing the observed shift of the MBSL Cr* lines to the ballistic compressor data and extrapolating to temperatures observed during cavitation (4700 K), we determined pressures of 300 ± 30 bar. Because the ballistic compressor data showed that the degree of Cr* line red shift decreased with increasing temperature, the pressure of 300 bar was taken as a lower limit.

Quantitative studies of the conditions generated during multibubble acoustic cavitation have benefited greatly from the observation of discrete atomic and molecular emission lines in MBSL spectra. This work has not only corroborated earlier work that

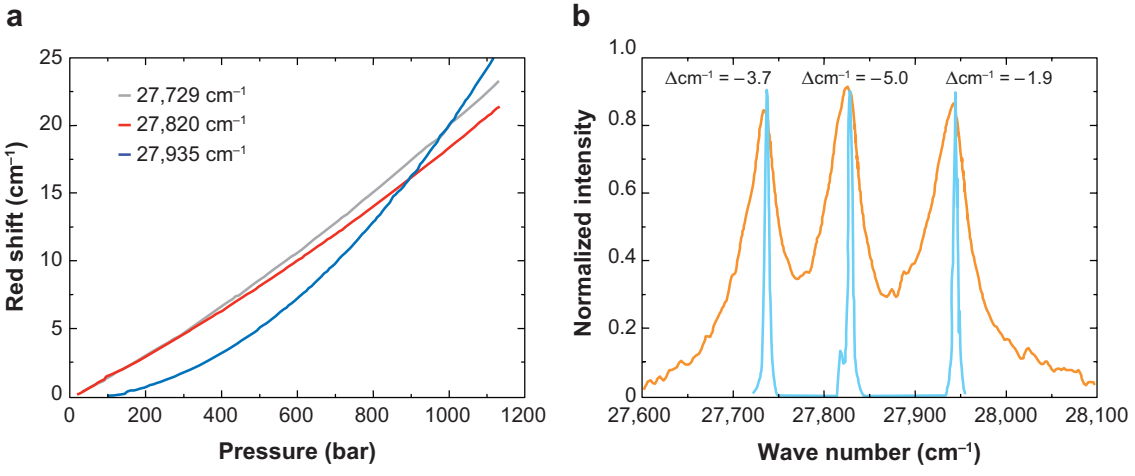

Figure 5

(*a*) Dependence of the peak positions of emission lines of Cr* atoms on the pressure of a bath gas of Ar at 3230 K. The wave number labels indicate the peak positions of the Cr* emission lines under ambient conditions. (*b*) Comparison of the multibubble sonoluminescence (MBSL) Cr* emission lines (*orange*) with the Cr* emission lines from a low-pressure hollow cathode lamp (*light blue*). Each MBSL Cr* line is labeled with its energy shift (red shift) relative to the hollow cathode lamp lines. For these observed shifts, the corresponding pressures (after extrapolation to 4700 K via the ideal gas law) are, from left to right, 240, 320, and 310 bar.

relied on more complicated methods having high degrees of uncertainty, it has also helped to clearly delineate the conditions generated during MBSL. Furthermore, a better understanding of sonochemical reaction mechanisms follows from having knowledge of the reaction conditions. For example, by quantifying the heating and cooling rates within a cavitating bubble ($\sim 10^{12}$ K s^{-1}), we can explain the formation of amorphous iron from the sonication of solutions of $Fe(CO)_5$: Cooling rates are sufficient to cause solidification before crystallization can occur (60).

Bjerknes force: acoustic radiation force felt by a bubble or particle in a sound field

SINGLE-BUBBLE SONOLUMINESCENCE

A single sonoluminescing bubble can be generated in a liquid that has been partially degassed and is irradiated with a standing acoustic wave of modest pressure (~1.5 atm) (17, 66, 67). Typically, spontaneous cavitation does not occur under these conditions at these modest acoustic pressures. Therefore, a bubble must be seeded by some external method (e.g., by putting a short current pulse through a nichrome wire to induce transient boiling, by perturbing the liquid surface with a small jet of water to entrain air bubbles, or by rapidly forming a vapor cavity via a focused laser pulse). Because the fundamental frequency of a standing acoustic wave generates a pressure antinode (velocity node) at approximately the center of the resonator, seeded bubbles quickly coalesce at the center of the flask, forming a single oscillating bubble. Due to the balance between the Bjerknes force (i.e., acoustic radiation force) and the buoyancy force (26), the bubble is (more or less) spatially stationary, but oscillates radially, in sync with the acoustic field (see **Figure 1**).

A single bubble trapped at the pressure antinode of the standing acoustic wave can be driven into highly nonlinear oscillations and made to emit brief flashes of broadband light. The spectral distribution of the light typically extends from the near infrared to the mid-ultraviolet and increases in intensity at higher frequencies (**Figure 6**) (19). Analyses of the brief light flashes and the accompanying bubble dynamics have revealed remarkable properties. Using time-correlated single-photon counting, researchers have found that the pulse width of the light flash can last anywhere from ~35 to 350 ps for a single bubble in water (68, 69). Furthermore, by using light scattering and Mie theory, researchers have found that the single bubble contracts by more than a factor of 100 within a few microseconds during implosion, reaching velocities of Mach 4 (relative to the ambient gas) and having accelerations at the turnaround point of 10^{11} *g* (27–28). More recent work in nonvolatile liquids such as sulfuric (H_2SO_4) and phosphoric (H_3PO_4) acid has found that, although the light flashes can be several nanoseconds in duration, the bubble implosion is much slower than that in water (70) but with several thousand-fold greater light emission (22). For shake tubes containing H_3PO_4, the flashes can reach microsecond durations but with lazy bubble collapse (71). This apparent paradox contradicts the shockwave model of SBSL (72) and remains unresolved.

Conditions During Single-Bubble Acoustic Cavitation

The typical emission spectrum observed during SBSL from water is characterized by a featureless continuum devoid of any lines or bands (19). This presents a problem

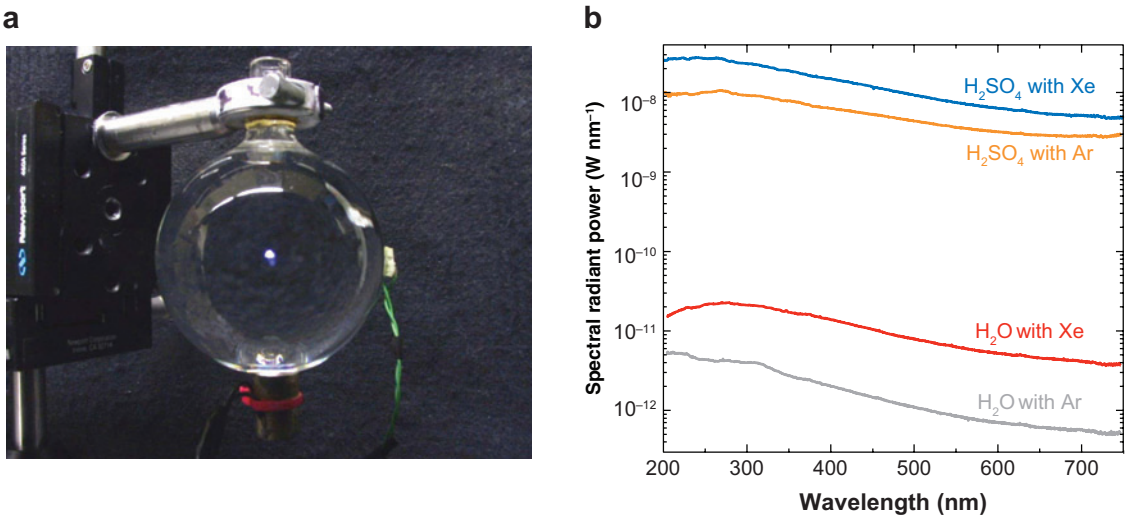

Figure 6

(*a*) Photograph of single-bubble sonoluminescence (SBSL) (*center white spot*), generated in 85 wt% H_2SO_4 partially regassed with Xe. The diameter of the spherical quartz cell is 6 cm. The exposure time was 2 s, and the photograph was taken in a fully lit room. (*b*) SBSL spectra from degassed water partially regassed with Ar or Xe compared to 85 wt% H_2SO_4. The applied acoustic pressure was optimized to give the maximum spectral radiant power for each.

when attempting to identify the species or mechanisms ultimately responsible for the light emission. Regardless, it is generally thought that the light emission arises from some combination of plasma processes (e.g., bremsstrahlung and ion-electron recombination), blackbody radiation, and pressure-broadened discrete electronic transitions (21, 73–77). Because of the inherent ambiguity associated with the analysis of featureless spectra of unknown origin, a more rigorous explanation is unlikely to be generated from SBSL spectra in water. Nevertheless, because of the remarkably short pulse widths, large bubble wall velocities and accelerations, and featureless spectra, much speculation has arisen regarding the intracavity conditions generated during SBSL (78, 79). Indeed, Taleyarkhan et al. (80, 81) published (controversial) claims of the experimental observation of signatures of thermonuclear fusion during acoustic cavitation; the experimental results on which such claims of sonofusion were made, however, have been thoroughly challenged (82–85).

Temperatures During Single-Bubble Sonoluminescence

The remarkable properties of the SBSL flash, the single-bubble dynamics, and the featureless emission spectra have made quantification of the conditions during bubble compression of wide interest. SBSL, however, is not as amenable as MBSL to the methods used for temperature and pressure measurements (i.e., kinetic or spectroscopic): First, a single bubble has a volume of only a few attoliters, so the concentrations of sonolysis products are very low and thus difficult to analyze (57); second, the

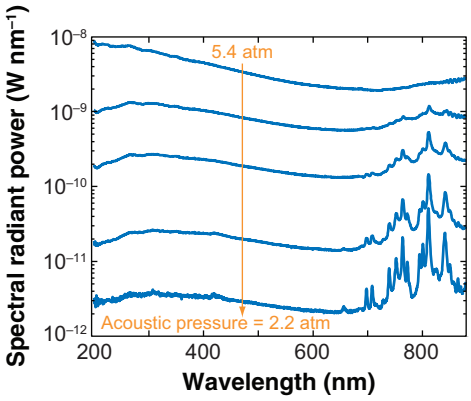

Figure 7

Single-bubble sonoluminescence as a function of P_a for 85 wt% H_2SO_4 partially regassed with Ar. The emission lines in the near infrared arise from excited state to excited state transitions within the Ar 4*p* – 4*s* manifold. The energies of the 4*p* levels range 12.9 to 13.4 eV, whereas the energies of the 4*s* levels range 11.5 to 11.8 eV.

intensity of SBSL light emission is usually low, and the emission spectra are typically featureless, which makes spectroscopic analysis difficult. Although there have previously been a few hints of molecular emission during SBSL, these spectra were not of the quality suitable for quantitative analysis (21, 76, 86).

We recently discovered that the radiant power generated during SBSL from H_2SO_4 is several thousand-fold larger than that previously observed from any other liquid (**Figure 6**) (22). In addition, the light flash from a single bubble in a shake tube of H_3PO_4 was found to comprise up to 10^{12} photons, a factor of roughly one million larger than that observed from water (71). Spectral analyses of SBSL from H_2SO_4 revealed emission lines from atoms, molecules, and ions originating from the liquid and from gas dissolved in the liquid (**Figure 7**) (87, 88). The observation of emission lines from ions provided the first definitive experimental evidence for the generation of a plasma during SBSL. In addition, the observation of strong discrete emission lines provided a means to determine the intracavity temperatures in the same manner as we did for MBSL. The fact that SBSL is generated from a single solitary bubble provides a significant advantage over MBSL; the system is not complicated by volume emission or scattering, and the bubble motion is not perturbed by interactions with other bubbles or the container walls.

The gas contents of a bubble during SBSL are primarily a noble gas. Research has shown that by dissolving a noble gas into solution, the SL intensity is significantly increased relative to other gases such as N_2 or O_2 (19, 20, 89). In addition, even if a small fraction of noble gas is mixed with a diatomic gas and dissolved into solution (or even air itself, which is 0.9% Ar), the SBSL from water behaves similarly to that observed from water containing the pure noble gas only. This is because the reactive diatomic gases are dissociated in the hot bubble interior and form soluble species (e.g., NO_x); the sonolysis products dissolve into the surrounding liquid, leaving only noble gas inside the bubble (57, 90–95). The low thermal conductivities of the heavier

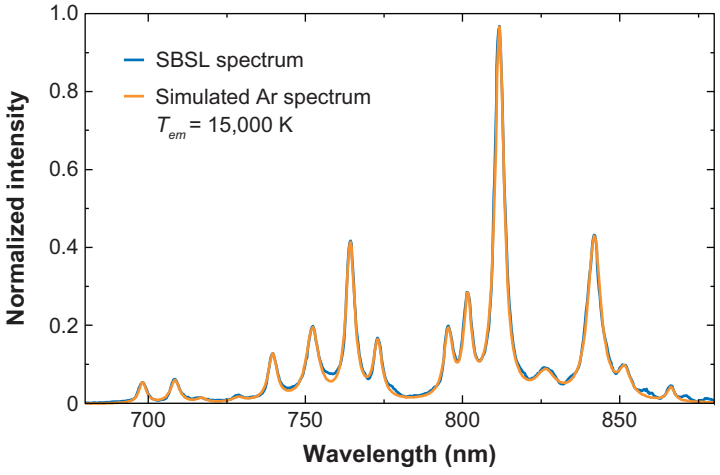

Figure 8

Single-bubble sonoluminescence (SBSL) from 85 wt% H_2SO_4 partially regassed with Ar. The emission lines arise from Ar* atoms. The SBSL emission is compared to a least-squares simulation of thermally equilibrated Ar* atom emission at 15,000 K. The underlying continuum has been subtracted for clarity.

noble gases as well as the high value of the polytropic ratio ($\gamma = 1.67$) also contribute to the observation of bright SL in the presence of these gases (7).

Although the use of noble gases is nearly ubiquitous in SL studies, emission from electronically excited noble-gas atoms was not observed until our recent work in mineral acids (22, 87). The observation of emission lines from noble-gas atoms, especially Ne and Ar whose excited states are 10 to 20 eV above the ground state, strongly suggests that a plasma was formed and was at least partly responsible for the light emission. The formation of a plasma during SBSL was verified on the direct observation of relatively weak emission lines from noble-gas monocations (Ar^+, Kr^+, and Xe^+) (88). By using the same technique as that employed for MBSL, one could then determine SBSL temperatures. By analyzing the relative intensities of the Ar* emission lines, we found temperatures of up to 15,000 K were generated during single-bubble cavitation (**Figure 8**). This temperature may not reflect the core temperature within the collapsing bubble: Plasma formation may lead to an optically opaque region within the bubble that is characterized by much higher temperatures and pressures; the observed temperature may well only reveal the conditions at the outer shell of the inner opaque core (22, 78, 79).

Pressures During Single-Bubble Sonoluminescence

Previous estimates of the pressures generated during SBSL have been made from modeling bubble motion during single-bubble cavitation (i.e., the radius-time curves calculated with an RPE and coupled to a simple model of adiabatic compression with temperatures estimated from the assumption of a blackbody radiator) (28). These

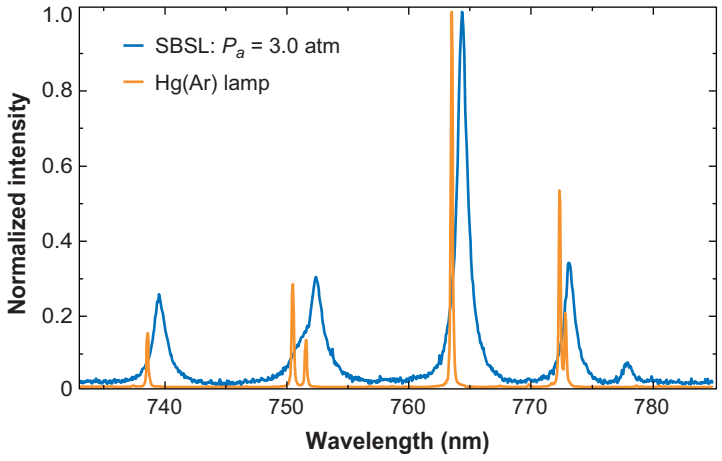

Figure 9

Comparison of the Ar* emission observed during single-bubble sonoluminescence (SBSL) (*blue*) in 85 wt% H_2SO_4 partially regassed with Ar with a low-pressure Hg(Ar) calibration lamp (*orange*). The configuration of the spectrograph was not adjusted between acquisitions. The underlying continuum has been subtracted for clarity. Note that the weak SBSL line at 777 nm results from the emission from electronically excited oxygen atoms.

assumptions give a highly model-dependent estimate of the pressure reached at R_{min}; calculated pressures of ~8000 atm were given for SBSL in water.

Alternatively, the standard tools of plasma diagnostics provide a complimentary method for determining the pressure from Ar* emission line profiles and have been used recently to determine experimentally the intracavity pressures during SBSL (23). Several mechanisms can contribute to the profile of an emission line from an electronically excited atom (58, 62–64). Depending on the conditions, some of these mechanisms contribute significantly less than others. During SBSL, for example, Doppler broadening can be assumed to be negligible, given the short mean-free path of the radiator relative to the wavelength of the emitted photon (96). For the Ar* emission lines observed during SBSL from H_2SO_4, it is assumed that only pressure broadening, the Stark effect, and instrument response are of significant enough importance to be considered. **Figure 9** compares the SBSL Ar* line profiles and peak positions with Ar* lines observed from a Hg(Ar) discharge lamp. As shown, the SBSL Ar* lines are significantly broadened and red shifted relative to the lamp lines, indicating the generation of high densities during bubble implosion.

Quantitative analysis of the densities and pressures generated during SBSL must begin by first isolating the broadening due to pressure from that due to Stark effects and instrument response. The Ar* 763.51-nm line is ideal for analysis as it is both intense and isolated from other lines. The full width at half maximum of the SBSL Ar* 763.51-nm line was found to be 1.0 nm via fitting with a pseudo-Voigt function, whereas the lamp line was 0.17 nm. Because we cannot assume that the instrument response is statistically independent from the other broadening mechanisms, deconvolution is necessary. Broadening due to pressure effects leads to a Lorentzian line

shape, whereas broadening due to the instrument response leads to a Gaussian line shape. Deconvolution can then be done using the expression derived by Whiting (97):

$$w_v = \frac{w_l}{2} + \sqrt{\left(\frac{w_l^2}{4} + w_g^2\right)}, \tag{6}$$

where w_v, w_l, and w_g represent the Voigt, Lorentzian, and Gaussian line widths, respectively. In the present case, the total line width (Voigt) and the instrument line width (Gaussian) are known, so we can solve Equation 6 for the Lorentzian component, which consists of pressure broadening and Stark effects. As typically done in plasma diagnostics, the SBSL line broadening due to Stark effects can simply be subtracted from the remaining line width to extract the pressure broadening (64). To determine the contribution by the Stark effect, we used an empirical approach first described by Jones et al. (98, 99). From this, the electron density and thus contribution by the Stark effect could be estimated.

Once the contribution to the total SBSL line width by pressure broadening is determined, we can determine the intracavity density via

$$\Delta\nu = \sqrt{\frac{8kT}{\pi^3 \mu_{Ar}}} \cdot \sigma_{Ar} \cdot n_{Ar}, \tag{7}$$

where $\Delta\nu$ is the line width; k is the Boltzmann constant; T is the SBSL temperature; μ_{Ar} is the reduced mass of the Ar collision partners; σ_{Ar} is the collision cross section for Ar defined as $\pi(2r_{Ar})^2$, where r_{Ar} is the Ar van der Waals radius; and n_{Ar} is the Ar density. Solving Equation 7 for n_{Ar} at an SBSL temperature of 10,000 K gives a density of 10^{21} Ar atoms per cubic centimeter for modest acoustic pressures. Application of the van der Waals equation of state to the determined Ar density and temperature then gives an SBSL pressure of 1400 bar. This density and pressure match well with those determined from a coupling of the measured bubble dynamics and an adiabatic compression model (23). At elevated P_a, where the Ar lines become broadened to the point of being indistinguishable from the underlying continuum, the bubble dynamics method estimates increased pressures of ~4000 bar.

CONCLUSIONS

Acoustic cavitation is a unique means to drive chemical reactions. Researchers have determined the intracavity conditions via both kinetic and spectroscopic methods. Spectroscopic methods of pyrometry have proven particularly formidable for temperature determinations during MBSL and SBSL. By employing the two-line radiance ratio method to relative intensities of emission lines from electronically excited metal atoms, we have determined an MBSL temperature of ~5000 K. From the wavelength shifts of metal-atom emission lines, we have also determined pressures of a few hundred bar.

Cavitation in a single, isolated bubble is generally assumed to be more intense than in a dense cloud of bubbles, owing to the sphericity of collapse and the lack of perturbation by other bubbles and the container walls. The recent observation of

emission lines from electronically excited Ar atoms in SBSL in nonaqueous liquids permits the determination of SBSL temperatures and pressures, in much the same manner as was done for MBSL. By comparing relative intensities of Ar* lines, we can determine emission temperatures and control them as a function of driving acoustic pressure up to 15,000 K. From profiles and widths of Ar lines, we determined SBSL pressures of 1400 bar. These pressures and temperatures were determined at modest P_a. At elevated P_a at which the Ar lines become severely broadened and indistinguishable from the underlying continuum, temperatures can be expected to be significantly higher, and pressures estimated from bubble dynamics and adiabatic compression are ~4000 bar.

These measured conditions may only hint at what occurs in the core of a collapsing bubble. Emission during single-bubble cavitation from noble-gas excited states as much as 20 eV above the ground state and plasma emission from Ar^+, Kr^+, and Xe^+ as much as 40 eV above the ground state suggest the presence (at least in some liquids under some conditions) of a transient, hidden, optically opaque core of higher energy still.

SUMMARY POINTS

1. Acoustic cavitation provides a unique means with which to drive chemical reactions (sonochemistry) and also can result in light emission (SL). The high temperatures and pressures and short lifetimes created at the end of implosive bubble collapse (i.e., the cavitation hot spot) can lead to the formation of interesting materials with unique properties. Quantification of the intracavity environment generated during bubble implosion is vital to gaining a better understanding of the reaction mechanisms at work. This has been done successfully with both the kinetic method via sonochemistry and spectroscopic methods via SL, with the spectroscopic methods proving to be quite formidable.
2. There are two distinct regimes of SL, MBSL and SBSL. MBSL is the light emission that occurs from a cloud of cavitating bubbles, whereas SBSL is the light emission that occurs from a single cavitating bubble. Spectroscopic analyses of MBSL have revealed that the light emission arises mainly from the radiative relaxation of electronically excited atoms and molecules with a relatively minor contribution from radiative plasma processes. The observation of emission bands from high-energy radical species shows that homolytic bond cleavage is significant during cavitation. Much higher temperatures and pressures are thought to be generated during SBSL relative to those generated during MBSL. This is because of the increased sphericity of the collapse, which arises from the isolation of the bubble from perturbations (e.g., other bubbles, liquid-gas interfaces, or the container walls).

3. Intensities, peak positions, and profiles of emission lines from electronically excited atoms and molecules have been used to quantify temperatures and pressures during both MBSL and SBSL. For example, we have used the relative intensities of Cr^* emission lines observed during MBSL to determine effective temperatures of ~5000 K, and their peak wavelengths to estimate pressures of ~300 bar. The relative intensities of emission lines observed from electronically excited Ar atoms during SBSL have been used to determine temperatures up to 15,000 K, and their profiles have been used to estimate pressures of well over 1000 atm.

DISCLOSURE STATEMENT

The authors are not aware of any biases that might be perceived as affecting the objectivity of this review.

ACKNOWLEDGMENTS

We wish to thank all of the Suslick group members, past and present, who have contributed over the past 30 years to our sonochemical and sonoluminescence studies. This work has been supported by the U.S. National Science Foundation and in part by the Defense Advanced Research Projects Agency.

LITERATURE CITED

1. Suslick KS, Didenko Y, Fang MM, Hyeon T, Kolbeck KJ, et al. 1999. Acoustic cavitation and its chemical consequences. *Philos. Trans. R. Soc. Lond. Ser. A* 357:335–53
2. Crum LA, Mason TJ, Reisse J, Suslick KS, eds. 1999. *Sonochemistry and Sonoluminescence*. AIP Conf. Proc. Vol. 524. Dordrecht: Kluwer Acad.
3. Suslick KS. 1990. Sonochemistry. *Science* 247:1439–45
4. Marinesco N, Trillat JJ. 1933. Action of supersonic waves upon the photographic plate. *C.R. Acad. Sci.* 196:858–60
5. Frenzel H, Schultes H. 1934. Luminescence in water carrying supersonic waves. *Z. Phys. Chem.* 27:B421–24
6. Taylor KJ, Jarman PD. 1970. The spectra of sonoluminescence. *Aust. J. Phys.* 23:319–34
7. Young FR. 1976. Sonoluminescence from water containing dissolved gases. *J. Acoust. Soc. Am.* 60:100–4
8. Neppiras EA. 1980. Acoustic cavitation. *Phys. Rep.* 61:159–251
9. Prosperetti A, Lezzi A. 1986. Bubble dynamics in a compressible liquid. Part 1. First-order theory. *J. Fluid Mech.* 168:457–78
10. Crum LA, Reynolds GT. 1985. Sonoluminescence produced by "stable" cavitation. *J. Acoust. Soc. Am.* 78:137–39

11. Walton AJ, Reynolds GT. 1984. Sonoluminescence. *Adv. Phys.* 33:595–660
12. Suslick KS, Flint EB. 1987. Sonoluminescence of non-aqueous liquids. *Nature* 330:553–55
13. Flint EB, Suslick KS. 1989. Sonoluminescence from nonaqueous liquids: emission from small molecules. *J. Am. Chem. Soc.* 111:6987–92
14. McNamara WB III, Didenko YT, Suslick KS. 1999. Sonoluminescence temperatures during multi-bubble cavitation. *Nature* 401:772–75
15. Flint EB, Suslick KS. 1991. The temperature of cavitation. *Science* 253:1397–409
16. McNamara WB III, Didenko YT, Suslick KS. 2003. Pressure during sonoluminescence. *J. Phys. Chem. B* 107:7303–6
17. Gaitan DF, Crum LA, Church CC, Roy RA. 1992. Sonoluminescence and bubble dynamics for a single, stable, cavitation bubble. *J. Acoust. Soc. Am.* 91:3166–83
18. Barber BP, Putterman SJ. 1991. Observation of synchronous picosecond sonoluminescence. *Nature* 352:318–20
19. Hiller R, Weninger K, Putterman SJ, Barber BP. 1994. Effect of noble gas doping in single-bubble sonoluminescence. *Science* 266:248–50
20. Hiller R, Putterman SJ, Barber BP. 1992. Spectrum of synchronous picosecond sonoluminescence. *Phys. Rev. Lett.* 69:1182–84
21. Didenko YT, McNamara WB III, Suslick KS. 2000. Molecular emission from single-bubble sonoluminescence. *Nature* 407:877–79
22. Flannigan DJ, Suslick KS. 2005. Plasma formation and temperature measurement during single-bubble cavitation. *Nature* 434:52–55
23. Flannigan DJ, Hopkins SD, Camara CG, Putterman SJ, Suslick KS. 2006. Measurement of pressure and density inside a single sonoluminescing bubble. *Phys. Rev. Lett.* 96:204301
24. Young FR. 1999. *Cavitation*. London: Imperial Coll. Press
25. Brennen CE. 1995. *Cavitation and Bubble Dynamics*. New York: Oxford Univ. Press
26. Matula TJ. 1999. Inertial cavitation and single-bubble sonoluminescence. *Philos. Trans. R. Soc. Lond. Ser. A* 357:225–49
27. Weninger KR, Barber BP, Putterman SJ. 1997. Pulsed Mie scattering measurements of the collapse of a sonoluminescing bubble. *Phys. Rev. Lett.* 78:1799–802
28. Weninger KR, Evans PG, Putterman SJ. 2000. Time correlated single photon Mie scattering from a sonoluminescing bubble. *Phys. Rev. E* 61:R1020–23
29. Moss WC. 1997. Understanding the periodic driving pressure in the Rayleigh-Plesset equation. *J. Acoust. Soc. Am.* 101:1187–90
30. Lohse D. 2003. Bubble puzzles. *Phys. Today* 56:36–41
31. Eddingsaas NC, Suslick KS. 2007. Evidence for a plasma core during multibubble sonoluminescence in sulfuric acid. *J. Am. Chem. Soc.* 129:3838–39
32. McNamara WB III, Didenko YT, Suslick KS. 2000. The nature of the continuum in multibubble sonoluminescence. *J. Am. Chem. Soc.* 122:8563–64
33. Bernstein LS, Zakin MR, Flint EB, Suslick KS. 1996. Cavitation thermometry using molecular and continuum sonoluminescence. *J. Phys. Chem.* 100:6612–19
34. Suslick KS, Price GJ. 1999. Applications of ultrasound to materials chemistry. *Annu. Rev. Mater. Sci.* 29:295–326

35. Adewuyi YG. 2005. Sonochemistry in environmental remediation. 1. Combinative and hybrid sonophotochemical oxidation processes for the treatment of pollutants in water. *Environ. Sci. Technol.* 39:3409–20
36. Hickenboth CR, Moore JS, White SR, Sottos NR, Baudry J, Wilson SR. 2007. Biasing reaction pathways with mechanical force. *Nature* 446:423–27
37. Prozorov T, Prozorov R, Suslick KS. 2004. High velocity inter-particle collisions driven by ultrasound. *J. Am. Chem. Soc.* 126:13890–91
38. Prozorov T, McCarty B, Cai Z, Prozorov R, Suslick KS. 2004. Effects of high-intensity ultrasound on $Bi_2Sr_2CaCu_2O_{8+x}$ superconductor. *Appl. Phys. Lett.* 85:3513–15
39. Doktycz SJ, Suslick KS. 1990. Interparticle collisions driven by ultrasound. *Science* 247:1067–69
40. Eddingsaas NC, Suslick KS. 2007. Intense mechanoluminescence and gas phase reactions from the sonication of an organic slurry. *J. Am. Chem. Soc.* 129:6718–19
41. Eddingsaas NC, Suslick KS. 2006. Mechanoluminescence: light from sonication of crystal slurries. *Nature* 444:163
42. Suslick KS, Hammerton DA, Cline RE. 1986. Sonochemical hot spot. *J. Am. Chem. Soc.* 108:5641–42
43. Henglein A, Kormann C. 1985. Scavenging of OH radicals produced in the sonolysis of water. *Int. J. Radiat. Biol.* 48:251–58
44. Kamath V, Prosperetti A, Egolfopoulos FN. 1993. A theoretical study of sonoluminescence. *J. Acoust. Soc. Am.* 94:248–60
45. Flannigan DJ, Suslick KS. 2007. Emission from electronically excited metal atoms during single-bubble sonoluminescence. *Phys. Rev. Lett.* 99:134301
46. Tauber A, Mark G, Schuchmann HP, von Sonntag C. 1999. Sonolysis of tert-butyl alcohol in aqueous solution. *J. Chem. Soc. Perkin Trans.* 2:1129–35
47. Hart EJ, Fischer CH, Henglein A. 1990. Sonolysis of hydrocarbons in aqueous solution. *Radiat. Phys. Chem.* 36:511–16
48. Rae J, Ashokkumar M, Eulaerts O, von Sonntag C, Reisse J, Grieser F. 2005. Estimation of ultrasound induced cavitation bubble temperatures in aqueous solutions. *Ultrason. Sonochem.* 12:325–29
49. Ciawi E, Rae J, Ashokkumar M, Grieser F. 2006. Determination of temperatures within acoustically generated bubbles in aqueous solutions at different ultrasound frequencies. *J. Phys. Chem. B* 110:13656–60
50. Ciawi E, Ashokkumar M, Grieser F. 2006. Limitations of the methyl radical recombination method for acoustic cavitation bubble temperature measurements in aqueous solutions. *J. Phys. Chem. B* 110:9779–81
51. Jeffries JB, Copeland RA, Suslick KS, Flint EB. 1992. Thermal equilibration during cavitation. *Science* 256:248
52. Didenko Y, McNamara WB III, Suslick KS. 1999. The temperature of multibubble sonoluminescence in water. *J. Phys. Chem. A* 103:10783–88
53. Lee J, Ashokkumar M, Kentish S, Grieser F. 2005. Determination of the size distribution of sonoluminescence bubbles in a pulsed acoustic field. *J. Am. Chem. Soc.* 127:16810–11

54. Tsochatzidis NA, Guiraud P, Wilhelm AM, Delmas H. 2001. Determination of velocity, size and concentration of ultrasonic cavitation bubbles by the phase-Doppler technique. *Chem. Eng. Sci.* 56:1831–40
55. Burdin F, Tsochatzidis NA, Guiraud P, Wilhelm AM, Delmas H. 1999. Characterisation of the acoustic cavitation cloud by two laser techniques. *Ultrason. Sonochem.* 6:43–51
56. Lauterborn W, Koch A. 1987. Holographic observation of period-doubled and chaotic bubble oscillations in acoustic cavitation. *Phys. Rev. A* 35:1974–76
57. Didenko YT, Suslick KS. 2002. The energy efficiency of formation of photons, radicals, and ions during single bubble cavitation. *Nature* 418:394–97
58. Ingle JD Jr, Crouch SR. 1988. *Spectrochemical Analysis*. Upper Saddle River, NJ: Prentice-Hall
59. Tourin RH. 1966. *Spectroscopic Gas Temperature Measurement: Pyrometry of Hot Gases and Plasmas*. New York: Elsevier
60. Suslick KS, Choe SB, Cichowlas AA, Grinstaff MW. 1991. Sonochemical synthesis of amorphous iron. *Nature* 353:414–16
61. Suslick KS, Flint EB, Grinstaff MW, Kemper KA. 1993. Sonoluminescence from metal carbonyls. *J. Phys. Chem.* 97:3098–99
62. Allard N, Kielkopf J. 1982. The effect of neutral nonresonant collisions on atomic spectral lines. *Rev. Mod. Phys.* 54:1103–82
63. Ch'en SY, Takeo M. 1957. Broadening and shift of spectral lines due to the presence of foreign gases. *Rev. Mod. Phys.* 29:20–73
64. Griem HR. 1997. *Principles of Plasma Spectroscopy*. New York: Cambridge Univ. Press
65. Holmes QA, Takeo M, Ch'en SY. 1969. Shift of the emission lines of chromium and nickel produced by argon and helium. *J. Quant. Spectrosc. Radiat. Transf.* 9:761–68
66. Brenner MP, Hilgenfeldt S, Lohse D. 2002. Single-bubble sonoluminescence. *Rev. Mod. Phys.* 74:425–84
67. Putterman SJ, Weninger KR. 2000. Sonoluminescence: how bubbles turn sound into light. *Annu. Rev. Fluid Mech.* 32:445–76
68. Hiller RA, Putterman SJ, Weninger KR. 1998. Time-resolved spectra of sonoluminescence. *Phys. Rev. Lett.* 80:1090–93
69. Gompf B, Günther R, Nick G, Pecha R, Eisenmenger W. 1997. Resolving sonoluminescence pulse width with time-correlated single photon counting. *Phys. Rev. Lett.* 79:1405–8
70. Hopkins SD, Putterman SJ, Kappus BA, Suslick KS, Camara CG. 2005. Dynamics of a sonoluminescing bubble in sulfuric acid. *Phys. Rev. Lett.* 95:254301
71. Chakravarty A, Georghiou T, Phillipson TE, Walton AJ. 2004. Stable sonoluminescence within a water hammer tube. *Phys. Rev. E* 69:066317
72. Wu CC, Roberts PH. 1993. Shock-wave propagation in a sonoluminescing gas bubble. *Phys. Rev. Lett.* 70:3424–27
73. Hammer D, Frommhold L. 2000. Spectra of sonoluminescent rare-gas bubbles. *Phys. Rev. Lett.* 85:1326–29
74. Vazquez G, Camara C, Putterman S, Weninger K. 2001. Sonoluminescence: nature's smallest blackbody. *Opt. Lett.* 26:575–77

75. Hilgenfeldt S, Grossmann S, Lohse D. 1999. A simple explanation of light emission in sonoluminescence. *Nature* 398:402–5
76. Young JB, Nelson JA, Kang W. 2001. Line emission in single-bubble sonoluminescence. *Phys. Rev. Lett.* 86:2673–76
77. Didenko YT, Gordeychuk TV. 2000. Multibubble sonoluminescence spectra of water which resemble single-bubble sonoluminescence. *Phys. Rev. Lett.* 84:5640–43
78. Moss WC, Clarke DB, Young DA. 1997. Calculated pulse widths and spectra of a single sonoluminescing bubble. *Science* 276:1398–401
79. Camara C, Putterman S, Kirilov E. 2004. Sonoluminescence from a single bubble driven at 1 megahertz. *Phys. Rev. Lett.* 92:124301
80. Taleyarkhan RP, West CD, Lahey RT, Nigmatulin RI, Block RC, Xu Y. 2006. Nuclear emissions during self-nucleated acoustic cavitation. *Phys. Rev. Lett.* 96:034301
81. Taleyarkhan RP, West CD, Cho JS, Lahey RT, Nigmatulin RI, Block RC. 2002. Evidence for nuclear emissions during acoustic cavitation. *Science* 295:1868–73
82. Shapira D, Saltmarsh M. 2002. Nuclear fusion in collapsing bubbles—Is it there? An attempt to repeat the observation of nuclear emissions from sonoluminescence. *Phys. Rev. Lett.* 89:104302
83. Tsoukalas L, Clikeman F, Bertodano M, Jevremovic T, Walter J, et al. 2006. Tritium measurements in neutron-induced cavitation of deuterated acetone. *Nucl. Technol.* 155:248–51
84. Naranjo B. 2006. Comment on "Nuclear emissions during self-nucleated acoustic cavitation". *Phys. Rev. Lett.* 97:149403
85. Camara CG, Hopkins SD, Suslick KS, Putterman SJ. 2007. Upper bound for neutron emission from sonoluminescing bubbles in deuterated acetone. *Phys. Rev. Lett.* 98:064301
86. Weninger KR, Cho H, Hiller RA, Putterman SJ, Williams GA. 1997. Sonoluminescence from an isolated bubble on a solid surface. *Phys. Rev. E* 56:6745–49
87. Flannigan DJ, Suslick KS. 2005. Molecular and atomic emission during single-bubble cavitation in concentrated sulfuric acid. *Acoust. Res. Lett. Online* 6:157–61
88. Flannigan DJ, Suslick KS. 2005. Plasma line emission during single-bubble cavitation. *Phys. Rev. Lett.* 95:044301
89. Barber BP, Wu CC, Löfstedt R, Roberts PH, Putterman SJ. 1994. Sensitivity of sonoluminescence to experimental parameters. *Phys. Rev. Lett.* 72:1380–83
90. Toegel R, Lohse D. 2003. Phase diagrams for sonoluminescing bubbles: a comparison between experiment and theory. *J. Chem. Phys.* 118:1863–75
91. Yasui K. 1997. Chemical reactions in a sonoluminescing bubble. *J. Phys. Soc. Jpn.* 66:2911–20
92. Lohse D, Hilgenfeldt S. 1997. Inert gas accumulation in sonoluminescing bubbles. *J. Chem. Phys.* 107:6986–97
93. Lohse D, Brenner MP, Dupont TF, Hilgenfeldt S, Johnston B. 1997. Sonoluminescing air bubbles rectify argon. *Phys. Rev. Lett.* 78:1359–62
94. Löfstedt R, Weninger K, Putterman S, Barber BP. 1995. Sonoluminescing bubbles and mass diffusion. *Phys. Rev. E* 51:4400–10

95. Flannigan DJ, Suslick KS. 2006. Plasma quenching by air during single-bubble sonoluminescence. *J. Phys. Chem. A* 110:9315–18
96. Dicke RH. 1953. The effect of collisions upon the Doppler width of spectral lines. *Phys. Rev.* 89:472–73
97. Whiting EE. 1968. An empirical approximation to Voigt profile. *J. Quant. Spectrosc. Radiat. Transf.* 8:1379–84
98. Jones DW, Wiese WL, Woltz LA. 1986. Ion broadening of Ar I lines in a plasma. *Phys. Rev. A* 34:450–56
99. Jones DW, Wiese WL. 1984. Asymmetry patterns of plasma-broadened isolated lines (C I). *Phys. Rev. A* 30:2602–8

Annual Review of
Physical Chemistry

Volume 59, 2008

Contents

Indexes

Errata

An online log of corrections to *Annual Review of Physical Chemistry* articles may be found at http://physchem.annualreviews.org/errata.shtml